

Antiproton-Hydrogen annihilation at sub-kelvin temperatures

A. Yu. Voronin

*P. N. Lebedev Physical Institute
53 Leninsky pr., 117924 Moscow, Russia*

J. Carbonell

*Institut des Sciences Nucléaires
53, Av. des Martyrs, 38026 Grenoble, France*

The main properties of the interaction of ultra low-energy antiprotons ($E \leq 10^{-6}$ a.u.) with atomic hydrogen are established. They include the elastic and inelastic cross sections and Protonium (Pn) formation spectrum. The inverse Auger process ($Pn + e \rightarrow H + \bar{p}$) is taken into account in the framework of an unitary coupled-channels model. The annihilation cross-section is found to be several times smaller than the predictions made by the black sphere absorption models. A family of $\bar{p}H$ nearthreshold metastable states is predicted. The dependence of Protonium formation probability on the position of such nearthreshold S-matrix singularities is analysed. An estimation for the $H\bar{H}$ annihilation cross section is obtained.

: 03.65.Nk; 34.10.+x, 11.80.J, 36.10.Dr

I. INTRODUCTION

The unique features of the LEAR (low-energy antiproton ring) facility at CERN made recently possible the synthesis of few antihydrogen atoms [1]. This effort would be pursued with the antiproton decelerator (AD) project [2] and would make possible the storage of sensible amounts of antihydrogen. This project reinforces the already active interest to investigate several theoretical and experimental problems in the physics of antimatter [3–7].

In view of storing antimatter in traps, it would be interesting to have some theoretical calculations of the rate at which antiprotons (\bar{p}) and antihydrogen (\bar{H}) annihilate with the residual gas. This process should be evaluated at subkelvin temperatures, the optimal energy domain for an effective synthesis and trapping of antimatter.

From a theoretical standpoint, a specific feature of systems like $H + \bar{p}$ or $H + \bar{H}$, containing pairs of unlike charged heavy particles (p and \bar{p}), is the possibility of rearrangement followed by Protonium (Pn) formation. Indeed even at zero \bar{p} kinetic energy Protonium can be produced in states with principal quantum number $n \leq 30$.

Since the pioneer work of E. Fermi and E. Teller [8] in 1947, this problem has been treated by several authors [9,10,12] in the energy range going from a fraction to tens a.u.. The usual approach is based on the following two assumptions: i) the separation of electronic and nuclear motion and ii) the classical treatment of the antiproton dynamics. The aim of the present work is to provide a correct description of the ultra-low energy limit, i.e. $T_{\bar{p}} < 10^{-6}$ a.u., an energy domain in which the above mentioned assumptions are no longer valid. As a consequence we are definitely faced to a quantum three- or four-body problem.

We will consider in what follows the annihilation of ultra slow antiprotons with atomic hydrogen in the framework of an unitary coupled channel approach. This process will be identified to the free Pn formation:

$$\bar{p} + H \rightarrow Pn^* + e \quad (1)$$

as far as the direct annihilation at such low energies can be neglected and that the further evolution of Pn states will result into annihilation.

In our treatment the Protonium formation as well as the virtual rearrangement process, i.e. the inverse reaction of (1):

$$\bar{p} + H \rightarrow Pn^* + e \rightarrow \bar{p} + H \quad (2)$$

will be properly taken into account.

We will show that the energy dependence of the inelastic reaction probability is determined by a rich spectrum of nearthreshold S-matrix singularities, corresponding to $H\bar{p}$ nearthreshold metastable states generated by the long range charge-dipole interaction. Finally we will give an estimation of the $H\bar{H}$ annihilation cross-section in the energy range from 10^{-8} to 10^{-4} a.u.

II. THE FORMALISM

The adequate formalism for the three-body problem are the Faddeev equations [13], according to which three possible asymptotic clusters have to be explicitly described. In the case of slow antiprotons scattering on hydrogen only two of them are physically important. The first one is the $(pe)\bar{p}$ cluster, which corresponds to the elastic channel $H + \bar{p} \rightarrow H + \bar{p}$. The second one is the $(p\bar{p})e$ cluster, corresponding to the Protonium formation channels $H + \bar{p} \rightarrow Pn^* + e$.

A direct solution of the Faddeev equations for such a problem is made difficult by the big number of open channels containing fast oscillating asymptotics. In this section we will develop a formalism which enables to take into account the correct behavior of the three-body wavefunction in both mentioned asymptotic clusters and benefit from the small value of the electron-antiproton mass ratio. We will show that this approach gives the scattering observables with an accuracy of the order of $\sim 10\%$ by using a very limited number of channels. In the same time it provides a transparent physical understanding of the low energy three-body dynamics in the $\bar{p}H$ reaction, which was the main aim of our study.

A. The coordinate system

The Jacobi coordinates for the 3-body problem are connected with the possible different asymptotic clusters. The coordinates corresponding to the elastic channel are defined by

$$\begin{aligned} \mathbf{r} &= \mathbf{r}_e - \mathbf{R}_p \\ \mathbf{R} &= \mathbf{R}_{\bar{p}} - \frac{m_e \mathbf{r}_e + M_p \mathbf{R}_p}{m_e + M_p} \end{aligned} \quad (3)$$

where \mathbf{r}_e , \mathbf{R}_p and $\mathbf{R}_{\bar{p}}$ are respectively the electron, proton and antiproton coordinates, and m_e M_p are the electron and proton mass.

It turns out that this frame is also convenient for describing the Protonium production channels. Indeed, the $p\bar{p}$ distance $\rho = \mathbf{R}_p - \mathbf{R}_{\bar{p}}$, coincides within $\mathbf{r}(m_e/M_p)$ with \mathbf{R} in equation (3). We will show that knowing the three-body wavefunction at $\mathbf{r} \ll \rho(M_p/m_e)$ is enough to get a good approximation of the scattering observables. Thus we can substitute ρ by \mathbf{R} and take into account, if necessary, the difference between ρ and \mathbf{R} in a perturbative way. We will use hereafter the unique coordinate system (3).

B. Three-body wavefunction

The three-body wavefunction is represented as a sum of two components, corresponding to the two considered clusters:

$$\Phi(\mathbf{r}, \mathbf{R}) = \Phi_1(\mathbf{r}, \mathbf{R}) + \Phi_2(\mathbf{r}, \mathbf{R}) \quad (4)$$

Component Φ_1 is supposed to describe the elastic channel and can be written as

$$\Phi_1(\mathbf{r}, \mathbf{R}) = \sum_{\alpha} \phi_{\alpha}(\mathbf{r}) \chi_{\alpha}(\mathbf{R}) \quad (5)$$

where α is the set of quantum numbers labeling the Hydrogen atomic states ϕ_{α} as well as the corresponding antiproton wavefunction χ_{α} . We will denote from now by channel each term in the three-body wavefunction expansion like (5).

For incident antiproton energy much smaller than the first Hydrogen excitation threshold, it is convenient to select from (5) only the contributions which do not vanish in the asymptotics. This gives the simple form:

$$\Phi_1(\mathbf{r}, \mathbf{R}) = \phi_{1s}(\mathbf{r}) \chi(\mathbf{R}) \quad (6)$$

It is useful to introduce a projection operator \hat{P} , which acts in the three-body states space and projects on the subspace of Hydrogen states corresponding to open channels:

$$\hat{P} = \sum_{nlm} |\phi_{nlm}\rangle \langle \phi_{nlm}| \otimes \hat{1} \quad (7)$$

In our case the sum is limited to the 1s state only. Component Φ_1 is then written as:

$$\Phi_1 = \hat{P}\Phi \quad (8)$$

The second component Φ_2 describes all the remaining channels and can be written in the form:

$$\Phi_2 = (\hat{1} - \hat{P})\Phi \quad (9)$$

This means that all the electron states except 1s contribute into Φ_2 ensuring the orthogonality of both components. The Φ_2 component contains terms which correspond to the Protonium formation channels. In order to explicitly take into account the asymptotic behavior of the cluster $(p\bar{p})e$, Φ_2 is expanded in a complete set of the $(p\bar{p})$ eigenfunctions $f_\beta(\mathbf{R})$:

$$\Phi_2(\mathbf{r}, \mathbf{R}) = \sum_{\beta} g_{\beta}(\mathbf{r}) f_{\beta}(\mathbf{R}) \quad (10)$$

where $g_{\beta}(\mathbf{r})$ are unknown expansion coefficients representing the electron wavefunctions in the channels characterized by Protonium quantum numbers β .

Let us remark here that at this level no approximation has been done. In particular the truncation done in the choice (6) of Φ_1 is balanced in the functions g_{β} of the second component.

C. Equations

The Schrodinger equation for a three-body vector state $|\Phi\rangle$ reads:

$$(\hat{H}_{ep} + \hat{H}_{p\bar{p}}^{ex} + \hat{W}_{e\bar{p}}^{ex} - E)|\Phi\rangle = 0 \quad (11)$$

with:

$$\hat{H}_{ep} = -\frac{1}{2m_e}\Delta_r - \frac{1}{r} \quad (12)$$

the Hydrogen Hamiltonian,

$$\hat{H}_{p\bar{p}}^{ex} = -\frac{1}{2M}\Delta_R - \frac{1}{|\mathbf{R} + \mathbf{r}(m_e/M_p)|} \quad (13)$$

the Protonium Hamiltonian and

$$\hat{W}_{e\bar{p}}^{ex} = \frac{1}{|\mathbf{R} - \mathbf{r}(1 - m_e/M_p)|} \quad (14)$$

the electron-antiproton interaction potential. M is the $\bar{p}H$ reduced mass which, neglecting m_e/M_p terms, will be hereafter approximated by the Protonium reduced mass $M \approx M_p/2$, $E = \varepsilon_B + E_{\bar{p}}$ the total energy, ε_B the Hydrogen ground state energy and $E_{\bar{p}}$ the center of mass energy of incident antiproton. Note that all the spin degrees of freedom are neglected. We will first neglect the term $\mathbf{r}(m_e/M_p)$ and substitute the exact $\hat{H}_{p\bar{p}}^{ex}$ and $\hat{W}_{e\bar{p}}^{ex}$ by the approximations:

$$\begin{aligned} \hat{H}_{p\bar{p}} &= -\frac{1}{2M}\Delta_R - \frac{1}{R} \\ \hat{W}_{e\bar{p}} &= \frac{1}{|\mathbf{R} - \mathbf{r}|} \end{aligned}$$

Using (8) and (9) we obtain the following coupled equations for the components $|\Phi_i\rangle$:

$$(\hat{H}_{p\bar{p}} + \hat{P}\hat{W}_{e\bar{p}}\hat{P} - E_{\bar{p}})|\Phi_1\rangle + \hat{P}\hat{W}_{e\bar{p}}(1 - \hat{P})|\Phi_2\rangle = 0 \quad (15)$$

$$(\hat{H}_{ep} + \hat{H}_{p\bar{p}} + (1 - \hat{P})\hat{W}_{e\bar{p}}(1 - \hat{P}) - E)|\Phi_2\rangle + (1 - \hat{P})\hat{W}_{e\bar{p}}\hat{P}|\Phi_1\rangle = 0$$

We used here the fact that \hat{P} commutes with \hat{H}_{ep} and $\hat{H}_{p\bar{p}}$.

The corresponding equations for the antiproton $\chi(R)$ and electron wave-functions $g_\beta(r)$ could be obtained by substituting (6) and (10) into (15). Due to the choice of the wavefunction components the solution of such a coupled equations system will correctly describe the asymptotic behavior of the three-body system. This procedure will however remain formal, for it leads to an infinite set of coupled channels, including the closed ones, characterized by a continuous $p\bar{p}$ momentum variable. To construct an equation system suitable for practical calculations, we should first analyze the contribution of different channels in the expansion (10). In particular, the one coming from the continuous spectrum. For such a purpose we represent Φ_2 as a sum of two components:

$$\Phi_2 = \Phi_2^d + \Phi_2^p \quad (16)$$

where

$$\Phi_2^d(\mathbf{r}, \mathbf{R}) = \hat{F}\Phi_2(\mathbf{r}, \mathbf{R}) = \sum_{\beta}^{n_{max}} g_\beta(\mathbf{r})f_\beta(\mathbf{R}) \quad (17)$$

$$\Phi_2^p(\mathbf{r}, \mathbf{R}) = (1 - \hat{F})\Phi_2(\mathbf{r}, \mathbf{R}) = \sum_{\beta=n_{max}}^{\infty} g_\beta(\mathbf{r})f_\beta(\mathbf{R}) \quad (18)$$

and

$$\hat{F} = \sum_{\beta}^{n_{max}} |f_\beta\rangle\langle f_\beta| \quad (19)$$

n_{max} is a certain set of Coulomb quantum numbers chosen in such a way, that Φ_2^d contains all the open channels and, eventually, a limited number of closed ones. The sum from n_{max} to infinity includes also the integration over the continuous \bar{p} momentum. The Φ_2^d component describes the dynamics of Protonium formation and includes the corresponding asymptotics of the three-body wavefunction :

$$\lim_{r \rightarrow \infty} \Phi_2^d(\mathbf{r}, \mathbf{R}) = \sum_{\beta} f_\beta(\mathbf{R}) S_\beta h_\beta^+(\mathbf{r})$$

Here S_β are the S-matrix elements for the Protonium formation and $h_\beta^+(r)$ are the outgoing electron waves in the channel with quantum numbers β . The component Φ_2^p contains only closed channels.

At big R the component Φ_2^d vanishes due to the Coulomb bound state wave functions f_β . On the contrary, the contribution from Φ_2^p is essential as far as it contains non vanishing terms coming from the $p\bar{p}$ states in the continuum corresponding to the virtual excitations and break-up. It is shown in Appendix that Φ_2^p actually describes the effect of the long-range polarization which can be taken into account by introducing in the elastic channel the local potential

$$V_{pol}(R) = \frac{1}{2} \frac{\alpha(R)}{R^4} \quad (20)$$

with $\alpha(R)$ ensuring that for $R \gg r_B$ (H-Bohr radius) $\alpha(R) \rightarrow -\alpha_d$ the H dipole polarizability. The following approximation [14] for $\alpha(R)$ was found to be suitable in practical calculations:

$$\alpha(R) = \frac{2}{3} \left(R^5 + \alpha_d R^4 + 2\alpha_d R^3 + \frac{3}{2}\alpha_d(R^2 + R + \frac{1}{2}) \right) e^{-2R} - \alpha_d$$

It is qualitatively shown in Appendix and proved by numerical calculations that at distances $R \approx r_B$, Φ_2^d dominates and the main contribution to the wavefunction comes from the channels with $n=26-40$, thus we can choose $V_{pol}(R \ll r_B) \rightarrow 0$.

We will first consider the case of total $H\bar{p}$ angular momentum L equal zero. The characteristic incident \bar{p} energy, below which S-wave dominates in the elastic channel will be determined later.

It was shown in [15,16] that in the $L = 0$ case, Protonium is primarily produced in states with angular momentum $l = 0$ and $l = 1$. The physical reason is that for the open channels with $n=26-30$, which dominate the reaction amplitude, the electron is ejected with rather small momentum k_e , and the centrifugal barrier reduces the probability to find a slow electron (and consequently Protonium) with high angular momentum.

The preceding results enable us to construct a model which, including a limited number of channels, correctly describes the asymptotic behavior of the three-body wavefunction. These channels dominate the reaction amplitude, while closed channels corresponding to the continuous spectrum of Protonium states, are taken into account by means of the polarization potential (20). In practical calculations we have included the Protonium channels with principal quantum number $n=10-40$ and angular momentum $l = 0, 1$. Numerical checks showed the stability of the results when increasing the number of included channels. The considered equation system has the form:

$$\left(-\frac{1}{2M}\partial_R^2 + \frac{L(L+1)}{2MR^2} + V_{cs}(R) + V_{pol}(R) - E + \varepsilon_B\right)\chi(R) + \sum_{n,l} \int \phi_{1s}(r)W_{0l}(r,R)f_{n,l}(R)\hat{\pi}g_{n,l}(r)dr = 0 \quad (21)$$

$$\sum_{n'l'} \left[\left(-\frac{1}{2m}\partial_r^2 - \frac{1}{r} + \frac{l(l+1)}{2mr^2} + E_n\right) \delta_{nn',ll'} + \hat{\pi}U_{nn',ll'}(r)\hat{\pi} \right] g_{n',l'}(r) + \hat{\pi}\phi_{1s}(r) \int f_{n,l}(R)W_{l0}(R,r)\chi(R) dR = 0 \quad (22)$$

Here :

$$V_{cs}(R) = -\left(1 + \frac{1}{R}\right)e^{-2R}$$

$$W_{0l}(r,R) = \begin{cases} r^l & r < R \\ r^{l+1} & r > R \end{cases} \frac{1}{\sqrt{2l+1}}$$

$$U_{nn',ll'} = \int f_{n,l}(\mathbf{R})f_{n',l'}(\mathbf{R})\frac{1}{|\mathbf{R}-\mathbf{r}|}d^3\mathbf{R}$$

$$\hat{\pi} = 1 - \hat{P}\delta_{0l}$$

and $E_n = -E + \frac{M}{2n^2}$

D. Effective potential method

The numerical solution of (21-22) is a rather difficult task, as far as each of the coupled integro-differential equations includes fast oscillating functions χ and f_n .

A way to overcome this difficulty is by means of the effective potential method. This approach turned to be an efficient tool for both a qualitative understanding and precise numerical treatment of the problem. The $H\bar{p}$ scattering observables are given by the first equation for antiproton wavefunction χ (21). The effects of the remaining coupled equations (22) are taken into account by transforming the system (21-22) into one equation for χ which contains a complex nonlocal effective potential:

$$\left(-\frac{1}{2M}\partial_R^2 + \frac{L(L+1)}{2MR^2} + V_{cs}(R) + \hat{V}_{eff} + V_{pol}(R) - E + \varepsilon_B\right)\chi(R) = 0 \quad (23)$$

with

$$\hat{V}_{eff} = \sum_{nn',ll'} |f_{n,l}\rangle\langle\phi_{1s}|W_{0l}(r,R)\hat{\pi}\hat{K}_{nn'}^{ll'}(r,r')\hat{\pi}W_{l0}(r',R')|\phi_{1s}\rangle\langle f_{n',l'}| \quad (24)$$

Here $\hat{K}_{nn'}^{ll'}(r,r')$ is the Green-matrix of coupled equation system for electron wave-functions:

$$\hat{K}_{nn'}^{ll'}(r,r') = \left\{ \left(-\frac{1}{2m}\partial_r^2 + \frac{l(l+1)}{2mr^2} + E_n - \frac{1}{r}\right) \delta_{nn'}^{ll'} + \hat{\pi}U_{nn'}^{ll'}\hat{\pi} \right\}^{-1} \quad (25)$$

The whole problem is then splitted into two parts: to calculate the effective potential and to solve the one-channel problem for antiproton scattering in a complex nonlocal potential.

The benefits of such an approach are several. On one hand the Green function (25) is calculated by solving a coupled equation system for smooth electron wavefunctions, while the fast oscillating $p\bar{p}$ wavefunctions are explicitly

introduced by the well-known Coulomb states. On the other hand the effective potential (24) practically does not depend on the \bar{p} incident energy in the domain $E_{\bar{p}} \ll 0.01$ a.u. [15,16]. The minimum energy of the ejected electron (from Pn state with $n=30$) is about 0.02 a.u. and for \bar{p} energies less than this value, the Green-matrix (25) is not sensitive to incident antiproton energy. This means that, once calculated for $E_{\bar{p}} = 0$, the effective potential can be used in the whole energy range of interest and this radically simplifies the calculations.

From a physical point of view it seems also more natural to analyze the properties of the $H\bar{p}$ system in terms of a modified one channel problem. The main features of the effective potential as they appear from our calculations are the following:

1. The imaginary part of V_{eff} vanishes at distance $R \approx 1.8r_B$, which corresponds to the mean radius of the last Protonium open channel ($n=30$). In Fig. 1 $Im[V_{eff}](R, R')$ for $R' = R$ is plotted as a function of R .
2. The imaginary part of $V_{eff}(R, R')$ is sharply peaked around its diagonal $R' = R$. Nevertheless for $R < r_B$, the nonlocality range is of the same order as the antiproton wavefunction $\chi(\mathbf{R})$ oscillation period. The profile of $Im[V_{eff}](R, R')$ for $R = 0.5$ is shown on Fig. 2.
3. The profile of the real part of V_{eff} is plotted in Fig. 3. Its nonlocality range is bigger than for the imaginary part. It vanishes at $R \approx 3r_B$ and dominates over the polarization V_{pol} and the Coulomb screened V_{cs} potentials in the range $1 < R < 3r_B$

III. RESULTS

In this section we will present the main results obtained in the coupled-channels model and discuss the physical reasons of certain scattering observables behavior.

A. Scattering observables

The $H\bar{p}$ complex scattering length is found to be:

$$a = (-7.8 - i11.5)r_B$$

The corresponding elastic cross-section at zero energy is:

$$\sigma_{el} = 2426.4r_B^2$$

We remark the relatively big value, in the atomic scale, of the scattering length imaginary part. Such value is a consequence of the long range polarization forces. By switching off V_{pol} in (23) the value obtained is substantially reduced to $Im(a) = 0.2r_B$. The capital role of the polarization forces in the low energy $H\bar{p}$ dynamics will be discussed in the next subsection.

We have calculated the energy dependence of the inelasticity S_r^2 for several partial waves. The results are shown on Fig. 4 for \bar{p} incident energies in the range from 0 to 10^{-6} a.u.. The inelasticity turns to be less than 0.1 for $E_{\bar{p}} < 10^{-8}$ a.u. and does not become greater than 0.5 in the energy domain of interest. One can also see in this figure that the scattering length approximation is valid for energies less than $10^{-8}a.u.$ The results for $l \neq 0$ have been calculated under the assumption that the effective potential (24) weakly depends on total angular momentum L in the energy range of interest. As one can see, S-wave dominates for $E_{\bar{p}} < 10^{-8}a.u.$.

The total annihilation cross-section is shown on Fig. 5. It follows the $1/v$ -law for $E_{\bar{p}} < 10^{-8}$ a.u. and decreases nonmonotonously for $E_{\bar{p}} > 10^{-8}$ a.u. Such nonmonotonic behavior is originated by the contribution of nonzero angular momentum partial waves, which is explicitly seen on Fig. 4. It is interesting to compare this cross-section with a semi-classical calculation [11] obtained under the following assumptions: i) the \bar{p} motion can be treated classically and ii) the annihilation takes place with unit probability as soon as the $\bar{p} - H$ distance is smaller than a critical radius $R_c = 0.64r_B$. The semi-classical cross-section, shown on Fig. 5, is approximately 2.5 times bigger than our values for $E_{\bar{p}} < 10^{-8}$ a.u. . This indicates that the low-energy $\bar{p}H$ annihilation is sensitive to the quantum dynamics of Protonium formation and could hardly be reproduced with models in which the details of such dynamics are not taken into account.

The population of different Protonium states, calculated for energies $E_{\bar{p}} < 10^{-8}a.u.$ is shown on Fig. 6. Protonium is produced primary in the S-states with principal quantum number $26 < n < 30$. The P-states population does not exceed 15% of the whole captured fraction of antiprotons. These results confirm our qualitative estimation concerning

the channels which give the main contribution into the reaction amplitude in the low-energy limit. It is worth to mention that Protonium S-states population dominates only for \bar{p} energies less than 10^{-8} a.u., while the population of states with higher l should increase with increasing energy [17].

We conclude this paragraph by emphasizing that the $H\bar{p}$ scattering observables significantly change their behavior at $E_{\bar{p}} \sim 10^{-8}$ a.u., a characteristic energy for the reaction. We will demonstrate that this behavior is determined by the presence of nearthreshold $H\bar{p}$ bound and virtual states generated by the polarization potential.

B. Nearthreshold metastable states

The polarization potential is known to significantly modify the low energy cross-sections of atomic reactions. It plays an essential role in the $H\bar{p}$ scattering. This potential produces a rich spectrum of $H\bar{p}$ weakly-bound and virtual states [18], which results from the long range character of the polarization forces and the heavy (in atomic scale) antiproton mass. Such states, being nearthreshold S-matrix singularities, determine the energy dependence of the $H\bar{p}$ scattering cross-section. The main properties of such states and their relation with the observables are discussed in this subsection.

We first remark that the polarization potential V_{pol} alone generates several \bar{p} weakly-bound states. The energy levels and mean radii of several nearest to the threshold S-states produced by V_{pol} alone are shown in Table I (values marked by subscript II). These states are extremely prolonged and have very small binding energies. By switching on the short range part of the interaction, i.e. the complex nonlocal effective potential V_{eff} and the screened Coulomb V_{cs} , the spectrum is modified and inelastic widths appear. Nevertheless, the main features, small binding energy ($10^{-8} < E_{bound} < 10^{-3}$ a.u.) and big radius ($4 < \bar{x} < 27$) r_B , remain.

In the threshold vicinity the elastic S-matrix for $L=0$ is dominated by its singularities and can be written in the form:

$$|S|(k) = \prod_i \frac{|k + z_i|}{|k - z_i|} \quad (26)$$

where z_i are the S-matrix poles with $Re(z_i) < 0$ due to $Im(V_{eff}) < 0$. In Fig. 7 are shown the trajectories of several S-matrix poles (P_i) and corresponding zeros (Z_i) as a function of the strength of the V_{eff} imaginary part. As it can be seen, the presence of the negative imaginary part in the effective potential results in shifting the S-matrix zeros to the right into the IV and I quadrants, with the corresponding symmetrical shift of S-matrix poles into the II and III ones. The position of the nearest to the origin S-matrix zero (and pole) corresponds to an energy of $E_c \sim 10^{-8}$ a.u. and plays a role of characteristic energy for the reaction (1). We notice however that this nearest to the threshold S-matrix singularity lies on the non-physical sheet, i.e. $Re(k) < 0$ and $Im(k) < 0$, and corresponds to a virtual state. Its wave function has an exponentially increasing asymptotic and does not represent a physical state.

As far as the usual definition of effective range can not be applied to the $1/R^4$ polarization potential [14], we introduce the characteristic range of $H\bar{p}$ interaction as: $R_A = 1/|k_0|$, where k_0 corresponds to the position of the nearest to the threshold S-matrix singularity. One can see, that for $k \geq k_0$ the scattering length approximation is no longer valid and higher order terms in the scattering amplitude expansion should be taken into account. With the result on Table I one gets $R_A \sim 103$ a.u. .

It is seen from (26) that for antiproton incident energies $E_{\bar{p}} \ll 10^{-8}$ a.u., $|k + z_i| \approx |k - z_i|$ and so $|S| \rightarrow 1$. This explains why the inelasticity S_r^2 for $E_{\bar{p}} \ll 10^{-8}$ a.u. turns to be much less than unit. For $E_{\bar{p}} \geq 10^{-8}$ a.u., and because there are several S-matrix zeros situated to the right from $-z_1$, one has $|k + z_i| < |k - z_i|$ and the reaction probability increases.

To illustrate how the position of the nearthreshold S-matrix singularities determines the low energy scattering, we have calculated the inelasticity as a function of the dipole polarizability α_d for a fixed energy ($E_{\bar{p}} = 10^{-8}$ and $E = 10^{-6}$ a.u.). This function is plotted on Fig. 8. The strong oscillations between its maximum and minimum values with decreasing α_d correspond to the motion of an S-matrix pole from the II to the III k-plane quadrant, while the symmetric S-matrix zero moves from the IV to the I quadrant. This means, that a weakly bound state becomes virtual. As it is seen from (26), the inelasticity reaches its maximum value when an S-matrix zero crosses the real k-axis.

This last result shows that sufficiently high accuracy of calculations is required to obtain the scattering length value. In the same time the reaction amplitude for energies $E_{\bar{p}} \gg 10^{-8}$ a.u. is less sensitive to the exact position of the nearthreshold singularities and can be more easily calculated. We estimate our accuracy in the scattering length results to be about 30%. This uncertainty appears mainly from approximation used for V_{pol} at short distances. To get more precise results one should increase the number of accounted closed channels and take into account the difference

between ρ and \mathbf{R} in (3). Such corrections seem not to be important for understanding the physics of the treated process and are beyond the scope of present paper.

We would like to emphasize that the nearthreshold character of mentioned S-matrix poles and zeros is determined by the long-range polarization potential. In the same time their exact position in complex k-plane can not be obtained without a proper treatment of the Protonium formation dynamics. In particular, the semiclassical black sphere condition does not hold in the energy domain $E_{\bar{p}} \leq 10^{-6}$ a.u. . In terms of S-matrix analytical properties the coupling with Protonium production channels produces comparatively big (for the energy domain of interest) shifts of the real part of the S-matrix zeros and reduces the inelasticity.

C. Local approximation of the effective potential

It was shown that the energy dependence of the reaction probability is determined by the existence of several nearthreshold states generated mainly by the long range polarization forces. This suggests the possibility to obtain a local complex potential which would be equivalent to the full $H\bar{p}$ interaction in the energy range of interest. By equivalent we mean not only to reproduce the same reaction probabilities but to support the same nearthreshold spectral structure as well.

We search for such equivalent local complex potential as a sum of three different terms

$$V_{loc}(R) = V_s(R) + V_{cs}(R) + V_{pol}(R)$$

$V_{cs}(R)$ and $V_{pol}(R)$ being respectively the Coulomb screened and polarization potential used in the previous section and V_s a local short rang part to be determined. It was assumed to have the form:

$$V_s(R) = \begin{cases} -V_1 e^{-\alpha_1 \left(\frac{R}{r_B}\right)} - i W_1 e^{-\beta_1 \left(\frac{R}{r_B}\right)} & \text{if } R < R_c \\ -i W_2 e^{-\beta_2 \left(\frac{R}{r_B}\right)} & \text{if } R \geq R_c \end{cases} \quad (27)$$

and a satisfactory fit is obtained with the following parameter values: $V_1 = 0.572$, $W_1 = W_2 = 0.040$, $\alpha_1 = 1.20$, $\beta_1 = \beta_2 = 3.20$ and $R_c = 2r_B$.

In Table II the results of calculations in nonlocal effective potential and mentioned above local approximation are compared. They agree within few percent accuracy in the energy range $0.5 \cdot 10^{-9} - 0.5 \cdot 10^{-6}$ a.u.

D. Hydrogen-Antihydrogen interaction

The results obtained for $H\bar{p}$ interaction can be used for a qualitative treatment of different atom-antiproton ($A\bar{p}$) and atom-antiatom ($A\bar{A}$) system.

It is of particular interest to estimate the $H\bar{H}$ annihilation cross-section, and thus to examine the reaction:



The $H\bar{H}$ system interacts at long distances via a dipole-dipole potential $V_{dd} \sim -6.5/R^6$. This potential also generates a spectrum of nearthreshold states. Some of them with $L=0$ are shown in Table III. In analogy with the (1) case one can expect that the corresponding S-matrix singularities will determine the (28) reaction dynamics.

A qualitative estimation of the $H\bar{H}$ potential can be obtained by adding to the same short-range part as in $H\bar{p}$ case the dipole-dipole long-range tail V_{dd} . The reaction (28) cross-section calculated in such a way is shown on Fig. 9. The characteristic energy for this reaction was found to be $\sim 10^{-5}$ a.u. , corresponding to the position of the nearest to the threshold S-matrix singularity (virtual state with energy $-7.8 \cdot 10^{-6}$ a.u.)

A similar treatment can be used to estimate the inelasticity energy dependence for different $A\bar{p}$ or $A\bar{A}$ systems in the low energy limit. For such a purpose one has to find the nearest to the threshold S-matrix singularity, generated by polarization potential. The necessary condition for the validity of such a qualitative approach is that the characteristic range R_A of the $A\bar{p}$ or $A\bar{A}$ long-range interaction should be much greater than the inelastic range r_A .

As it is seen from (24) the inelastic range is mainly determined by the mean radius of the last Protonium state open channel and thus given by:

$$\frac{M_A}{2n^2} = I_A$$

$$r_A \approx \frac{2n^2}{M_A} = \frac{1}{I_A}$$

where M_A and I_A are the $A\bar{p}$ reduced mass and the first ionization potential respectively, n is the principal quantum number of the last open channel. A similar estimation for the AA inelastic range $r_{A\bar{A}}$ can be obtained, if we take into account that Positronium is produced in this collision:

$$\begin{aligned}\frac{M_{A\bar{A}}}{2n^2} &= 2I_A - \varepsilon_{Ps} \\ \varepsilon_{Ps} &= I_H/2 \\ r_A &\approx \frac{2n^2}{M_{A\bar{A}}} = \frac{1}{(2I_A - I_H/2)}\end{aligned}$$

Here $M_{A\bar{A}}$ is the reduced mass of the $AA\bar{A}$ system, ε_{Ps} is the Positronium ground state energy.

Like in the $H\bar{p}$ case, the presence of nearthreshold virtual states may considerably increase the characteristic range of $A\bar{p}$ or $AA\bar{A}$ interaction. However it can be interesting to have a simple approximation of this range in the aim of comparison with preliminary estimations (see also [12]). This is provided by the semiclassical condition for the number N of states :

$$\int \sqrt{2M_A V_{pol}^A(R)} dR \approx \pi N$$

This condition may be rewritten as follows:

$$\frac{R_A}{r_B} \approx \pi N$$

For the $A\bar{p}$ case we obtain:

$$R_A \sim \begin{cases} \sqrt{2M_A C_4^A} & \text{if } L = 0 \\ \sqrt{2M_A C_4^A / L(L+1)} & \text{if } L > 0 \end{cases} \quad (29)$$

while for $AA\bar{A}$ one has:

$$R_A \sim \begin{cases} \sqrt[4]{2M_{A\bar{A}} C_6^A} & \text{if } L = 0 \\ \sqrt[4]{2M_{A\bar{A}} C_6^A / L(L+1)} & \text{if } L > 0 \end{cases} \quad (30)$$

C_4^A and C_6^A being the atom charge-dipole and dipole-dipole van der Waals constants. Finally, we get the following ratio of inelastic and polarization range:

$$\frac{r_A}{R_A} = \begin{cases} \frac{1}{I_A \sqrt{2M_A C_4^A}} & \text{if } L = 0 \\ \frac{\sqrt{L(L+1)}}{I_A \sqrt{2M_A C_4^A}} & \text{if } L > 0 \end{cases} \quad (31)$$

for atom-antiproton, and:

$$\frac{r_A}{R_A} = \begin{cases} \frac{1}{(2I_A - I_H/2) \sqrt[4]{2M_{A\bar{A}} C_6^A}} & \text{if } L = 0 \\ \frac{\sqrt[4]{L(L+1)}}{(2I_A - I_H/2) \sqrt[4]{2M_{A\bar{A}} C_6^A}} & \text{if } L > 0 \end{cases} \quad (32)$$

for atom-antiatom interaction.

The ratios (31-32), calculated for a wide range of different atoms, turns to be much smaller than unit in case $L=0$. In particular, for He, the less polarizable atom, they are ~ 0.02 for $He\bar{p}$, and ~ 0.05 for $He\bar{He}$. The polarization range dominates over the inelastic one in the partial waves up to $L \sim 10$ for $He\bar{p}$, and $L \sim 4$ for $He\bar{He}$. These values of L characterize the maximum angular momentum, which makes possible the existence of extended polarization states.

IV. CONCLUSION

A coupled channels model describing the $H\bar{p}$ system at energies less than 10^{-6} a.u. has been developed. The results thus obtained substantially differ from the low energy extrapolations of the black sphere model and other classical or

semiclassical approaches. They show that such a low energy requires a quantum mechanical treatment in which the dynamics of the Protonium formation is properly taken into account.

The effective $H\bar{p}$ optical potential has been calculated in the framework of the coupled channels model. In this framework, the $H\bar{p}$ scattering length and zero energy elastic cross section were found to be $a = (-7.8 - i11.5)r_B$ and $\sigma_{el} = 2426.4r_B^2$ respectively. The $H\bar{p}$ inelastic cross section has been calculated in the energy range from 10^{-9} to 10^{-6} a.u.. It follows the $1/v$ behavior up to energies $\sim 10^{-8}$ a.u. where the scattering length approximation is valid. The inelasticity turned to be much smaller than the black sphere model predictions.

The Protonium formation spectrum for the energies less than 10^{-8} a.u. has been calculated. We have shown that the population of S-states with principal quantum number from 26 to 30 accounts for 75% of the total captured fraction.

The reaction dynamics is found to be determined by the existence of several nearthreshold states. Such states are produced by the long-range polarization potential and are shifted in the complex momentum plane by the coupling with Protonium formation channels. The $H\bar{p}$ scattering length appears to be very sensitive to the position of the mentioned singularities and requires accurate calculations.

A local approximation of the effective potential has been proposed for further applications. It reproduces the scattering observables in the considered energy range and has the same nearthreshold spectral properties.

A qualitative extension of this approach to more general systems (atom- \bar{p} and atom-antiatom) has been discussed.

The results discussed in this work have been obtained within an approximate model. In view of them and motivated by the futur project of storing antimater at CERN it would be interesting to check the validity of the different approximations by developing more accurate treatments including an exact solution of the three body problem.

V. ACKNOWLEDGMENTS

The authors would like to thank I.S. Shapiro for suggesting the problem. One of the authors (A.V.) would like to thank D. Morgan for useful discussions.

APPENDIX A: APPENDIX

The aim of this appendix is to find the dominant channels in the expansion (10) of the three-body wavefunction. We first analyze the behavior of the component Φ_2^p at distances $R \gg r_B$. The equations system for Φ_2^d and Φ_2^p in terms of the projection operators \hat{P} (7) and \hat{F} reads: (19):

$$\begin{aligned} (\hat{H}_{p\bar{p}} + \hat{P}\hat{W}_{e\bar{p}}\hat{P} - E_{\bar{p}})|\Phi_1\rangle + \hat{P}\hat{W}_{e\bar{p}}(1 - \hat{P})\hat{F}|\Phi_2^d\rangle + \\ + \hat{P}\hat{W}_{e\bar{p}}(1 - \hat{P})(1 - \hat{F})|\Phi_2^p\rangle = 0 \end{aligned} \quad (\text{A1})$$

$$\begin{aligned} (\hat{H}_{ep} + \hat{H}_{p\bar{p}} + \hat{F}(1 - \hat{P})\hat{W}_{e\bar{p}}(1 - \hat{P})\hat{F} - E)|\Phi_2^d\rangle + \\ + \hat{F}(1 - \hat{P})\hat{W}_{e\bar{p}}(1 - \hat{P})(1 - \hat{F})|\Phi_2^p\rangle + (1 - \hat{P})\hat{F}\hat{W}_{e\bar{p}}\hat{P}|\Phi_1\rangle = 0 \end{aligned} \quad (\text{A2})$$

$$\begin{aligned} (\hat{H}_{ep} + \hat{H}_{p\bar{p}} + (1 - \hat{F})(1 - \hat{P})\hat{W}_{e\bar{p}}(1 - \hat{P})(1 - \hat{F}) - E)|\Phi_2^p\rangle + \\ + (1 - \hat{F})(1 - \hat{P})\hat{W}_{e\bar{p}}\hat{P}\hat{F}|\Phi_2^d\rangle + (1 - \hat{P})(1 - \hat{F})\hat{W}_{e\bar{p}}\hat{P}|\Phi_1\rangle = 0 \end{aligned} \quad (\text{A3})$$

By taking into account that at big R the projection operator \hat{F} vanishes, equations (A1-A3) simplify into the following system, valid for $R \gg r_B$:

$$(\hat{H}_{p\bar{p}} + \hat{P}\hat{W}_{e\bar{p}}\hat{P} - E_{\bar{p}})|\Phi_1\rangle + \hat{P}\hat{W}_{e\bar{p}}(1 - \hat{P})|\Phi_2^p\rangle = 0 \quad (\text{A4})$$

$$(\hat{H}_{p\bar{p}} + \hat{H}_{ep} + (1 - \hat{P})\hat{W}_{e\bar{p}}(1 - \hat{P}) - E)|\Phi_2^p\rangle + (1 - \hat{P})\hat{W}_{e\bar{p}}\hat{P}|\Phi_1\rangle = 0 \quad (\text{A5})$$

This system can be solved with respect to Φ_2^p and gives for the component Φ_1 :

$$(\hat{H}_{p\bar{p}} + \hat{P}\hat{W}_{e\bar{p}}\hat{P} - E_{\bar{p}})|\Phi_1\rangle + \hat{P}\hat{W}_{e\bar{p}}(1 - \hat{P})\hat{G}_{pol}(1 - \hat{P})\hat{W}_{e\bar{p}}\hat{P}|\Phi_1\rangle = 0 \quad (\text{A6})$$

in which

$$\hat{G}_{pol} = - \left(\hat{H}_{p\bar{p}} + \hat{H}_{ep} + (1 - \hat{P})\hat{W}_{e\bar{p}}(1 - \hat{P}) - E \right)^{-1} \quad (\text{A7})$$

The last term in equation (A6) is the polarization long-range interaction:

$$\hat{V}_{pol} = \langle \phi_{1s} | \hat{W}_{e\bar{p}}(1 - \hat{P}) \hat{G}_{pol} (1 - \hat{P}) \hat{W}_{e\bar{p}} | \phi_{1s} \rangle \quad (\text{A8})$$

The asymptotics of the Green-function \hat{G}_{pol} at $R, R' \gg r_B$ is:

$$G_{pol}(R, R', r, r') = \sum_{\alpha} \frac{1}{2p_{\alpha}} \left(e^{-p_{\alpha}|R-R'|} - S_{\alpha} e^{-p_{\alpha}(R+R')} \right) \phi_{\alpha}(r) \phi_{\alpha}(r')$$

where $p_{\alpha} = \sqrt{2M(|E - \varepsilon_{\alpha}|)}$ and α is a set of spherical Coulomb quantum numbers. If we take into account that at big R , \hat{V}_{pol} acts on the very slowly changing function $\chi(R)$ (the oscillation period of χ for $R \gg r_B$ is indeed much greater than r_B) we can substitute G_{pol} in (A8) by the following expression:

$$G_{pol}(R, R', r, r') = \delta(R - R') \sum_{\alpha} \frac{\phi_{\alpha}(r) \phi_{\alpha}(r')}{E - \varepsilon_{\alpha}}$$

By keeping terms up to $1/R^4$ we obtain the well-known charge-dipole potential asymptotic behavior:

$$V_{pol}(R \gg r_B) = -\frac{\alpha_d}{2R^4}$$

$$\alpha_d = -2 \sum_{\alpha \neq (1s)} \langle \phi_{1s} | \hat{d} | \phi_{\alpha} \rangle \frac{1}{\varepsilon_B - \varepsilon_{\alpha}} \langle \phi_{\alpha} | \hat{d} | \phi_{1s} \rangle \quad (\text{A9})$$

Here \hat{d} stands for the dipole momentum operator. One recognizes in (A9) the expression for the Hydrogen dipole polarizability, $\alpha_d = 9/2$. We can thus conclude that the contribution of Φ_2^p at big distances R can be taken into account by introducing in the elastic channel the polarization charge-dipole potential.

To qualitatively estimate the contribution of different channels at distances $R \approx r_B$ we first obtain the solution of (A1) in the distorted wave approximation. Component Φ_{1s}^0 , obtained by neglecting the coupling to other components, is $\Phi_1^0 = \phi_{1s}\chi^0$ with χ^0 satisfying the equation:

$$\left(-\frac{1}{2M} \partial_R^2 + V_{cs}(R) - E + \varepsilon_B \right) \chi^0 = 0$$

The contributions of components Φ_2^d and Φ_2^p are characterized by the integrals:

$$\langle \chi^0 \hat{P} | \hat{W}_{e\bar{p}}(1 - \hat{P}) | \hat{F} \rangle$$

$$\langle \chi^0 \hat{P} | \hat{W}_{e\bar{p}}(1 - \hat{P}) | (1 - \hat{F}) \rangle \quad (\text{A10})$$

An estimation of integrals (A10) can be obtained if we take into account the semiclassical character of the wavefunction χ^0 and the Coulomb wavefunctions at $R \approx r_B$ in expansions (17) and (18). We are dealing with an integral of fast-oscillating functions which has significant values only if there exist stationary phase points inside the integration region. The equation for such stationary phase points is:

$$\left(\frac{1}{R} + 1 \right) e^{-2R} = \frac{1}{R} - \frac{M}{2n^2}$$

It can be shown that there are no stationary phase points for Φ_2^p , while the contribution of Φ_2^d at the distance $R \approx r_B$ is mainly exhausted by Protonium states with principal quantum number $26 < n < 40$ (see [15,16]).

We have, in conclusion, that in the energy domain of interest and large internucleon distances the contribution of Φ_2^p is the only important one and can be taken into account by introducing the polarization potential (A8), while at the distances $R \approx r_B$ the component Φ_2^d dominates, and can be described by a limited number of channels. These qualitative arguments are important for construction of the first approximation, and should be proved by further numerical calculations.

- [1] G. Baur et al., Phys. Lett. **368B**, 251 (1996)
- [2] Fundamental studies of the antiproton at the AD, CERN/SPSLC 96-12/I207
In flight spectroscopy of antihydrogen at the proposed antiproton facility AD, SPSLC 96-25/M579
- [3] G. Gabrielse et al., Hyperfine Interactions **81**, 5 (1993).
- [4] G. Gabrielse et al., Hyperfine Interactions **89**, 371 (1994).
- [5] Proceedings of the Antihydrogen Workshop, Edited by J. Eades, Hyp. Int. **76** (1993)
- [6] M. Charlton et al, Phys. Rep. **241** 65 (1994)
- [7] Proceedings of the Low Energy Antiproton Physics LEAP'94, Edited by G. Kernel et al., World Scientific (1995)
- [8] E.Fermi, E.Teller, Phys. Rev. **72**, 399 (1947)
- [9] D.L. Morgan, Jr. and V.W. Hughes, Phys. Rev. D **2**, 1389 (1970)
W. Kolos, D.L. Morgan Jr. et. al Phys. Rev A **11**, 1792 (1975)
- [10] B.R. Junker and J.N. Bardsley, Phys. Rev. Lett. **28**, 1227 (1972)
- [11] D.L. Morgan, Jr. Hyperfine Interactions **44**,399 (1988)
- [12] G.V. Shlyapnikov et al., Hyperfine Interactions **76**, 31 (1993)
- [13] L.D. Faddeev Tr. Mat. Inst. Akad. Nauk SSSR **1**, 69 (1963)
- [14] N.F. Mott, H.S.W. Massey, The theory of atomic collisions, Oxford, Clarendon Press, (1965)
- [15] A.Yu. Voronin Sov. Phys. JETP **75** (3),416 (1992)
- [16] A. Yu. Voronin and J. Carbonell, Proceedings of the International School of Physics of Exotic Atoms, Molecules and Their Interactions, INFN/AE-94/24 , 281 (1994)
- [17] E. Borie, M. Leon, Phys. Rev. A **21**, 1460 (1980)
G. Reifenrother and E. Klempt, Nucl. Phys. **A503**, 885 (1989)
- [18] J. Carbonell, F. Ciesielski, C. Gignoux, A. Voronin, ISN Preprint 95.23 (1995), Few-Body Systems Suppl. **8**, 428 (1995)

E_I	E_{II}	\bar{x}_{II}
	$-5.1 \cdot 10^{-8} + i \cdot 7 \cdot 10^{-9}$	
$-4.2 \cdot 10^{-7}$	$-2.5 \cdot 10^{-6} - i \cdot 2 \cdot 10^{-7}$	27.0
$-3.6 \cdot 10^{-5}$	$-7.0 \cdot 10^{-5} - i \cdot 8.4 \cdot 10^{-6}$	11.3
$-2.6 \cdot 10^{-4}$	$-4.1 \cdot 10^{-4} - i \cdot 3.2 \cdot 10^{-5}$	7.3
$-9.2 \cdot 10^{-4}$	$-1.5 \cdot 10^{-3} - i \cdot 8.6 \cdot 10^{-5}$	5.3
$-2.3 \cdot 10^{-3}$	$-4.2 \cdot 10^{-3} - i \cdot 2.0 \cdot 10^{-4}$	4.2

TABLE I. Energies, Auger widths and mean radii (a.u) of L=0 $H\bar{p}$ states. We denote by index I the results in the V_{pol} alone and by index II those obtained with the full interaction ($V_{pol} + V_{cs} + V_{eff}$)

$E_{\bar{p}}$ (a.u.)	S_r^2 (I)	S_r^2 (II)	S (I)	S (II)
$0.5 \cdot 10^{-9}$	0.043	0.043	$0.978 + i0.01$	$0.978 + i0.014$
$0.5 \cdot 10^{-8}$	0.12	0.122	$0.937 + i0.013$	$0.936 + i0.021$
$0.5 \cdot 10^{-7}$	0.266	0.266	$0.836 - i0.185$	$0.836 - i0.177$
$0.5 \cdot 10^{-6}$	0.42	0.425	$0.023 - i0.756$	$0.034 - i0.757$

TABLE II. Inelasticity (S_r^2) and S-matrix (S) values calculated in the full effective potential (index I) and in its local approximation (index II) at different energies ($E_{\bar{p}}$)

E_I	E_{II}	\bar{x}_{II}
$-7.8 \cdot 10^{-6}$	$-6.1 \cdot 10^{-6} + i \cdot 1.8 \cdot 10^{-5}$	
$-1.9 \cdot 10^{-4}$	$-4.3 \cdot 10^{-4} - i \cdot 2.2 \cdot 10^{-4}$	4.6
$-2.9 \cdot 10^{-3}$	$-5.2 \cdot 10^{-3} - i \cdot 1.2 \cdot 10^{-3}$	2.8
$-1.1 \cdot 10^{-2}$	$-2.9 \cdot 10^{-2} - i \cdot 8.4 \cdot 10^{-3}$	1.5
$-3.3 \cdot 10^{-2}$	$-5.8 \cdot 10^{-3} - i \cdot 9.2 \cdot 10^{-3}$	1.3

TABLE III. Energies, Auger widths and mean radii (a.u) of L=0 $H\bar{H}$ states. We denote by index I the results in the V_{pol} alone and by index II those obtained with the full interaction ($V_{pol} + V_{cs} + V_{eff}$)

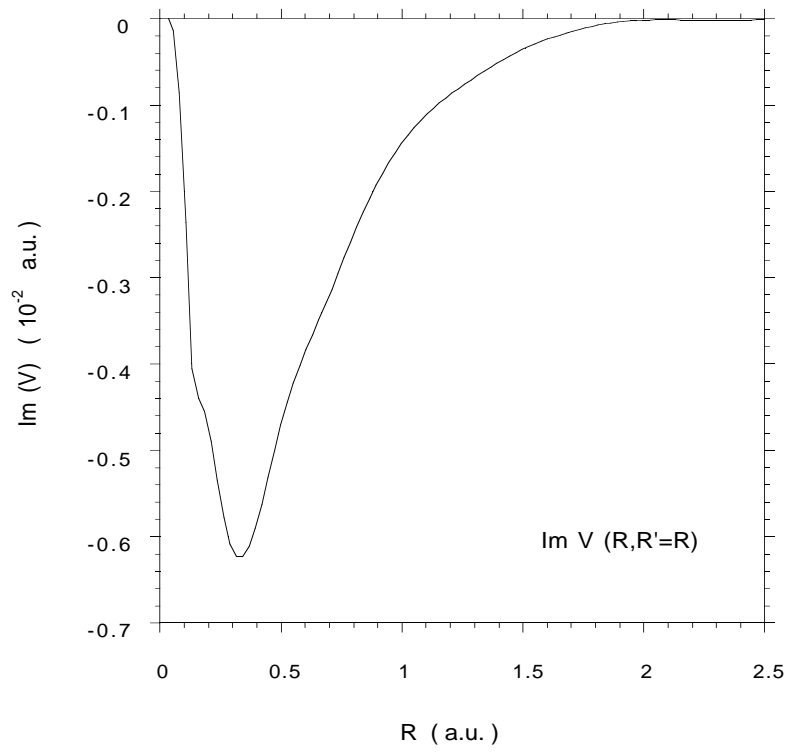


FIG. 1. Imaginary part of effective potential $V_{eff}(R, R' = R)$

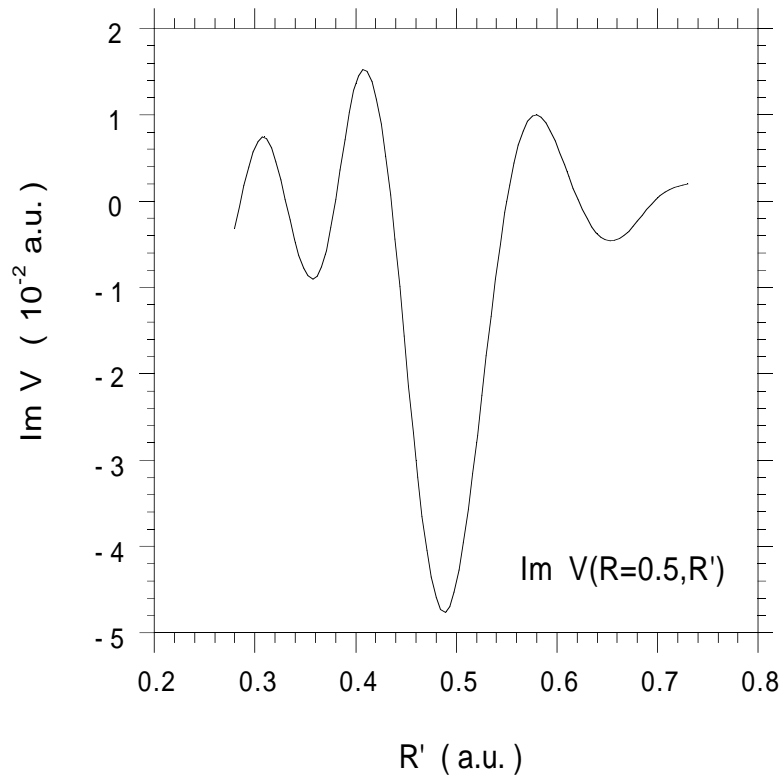


FIG. 2. Imaginary part of effective potential $V_{eff}(R = 0.5, R')$

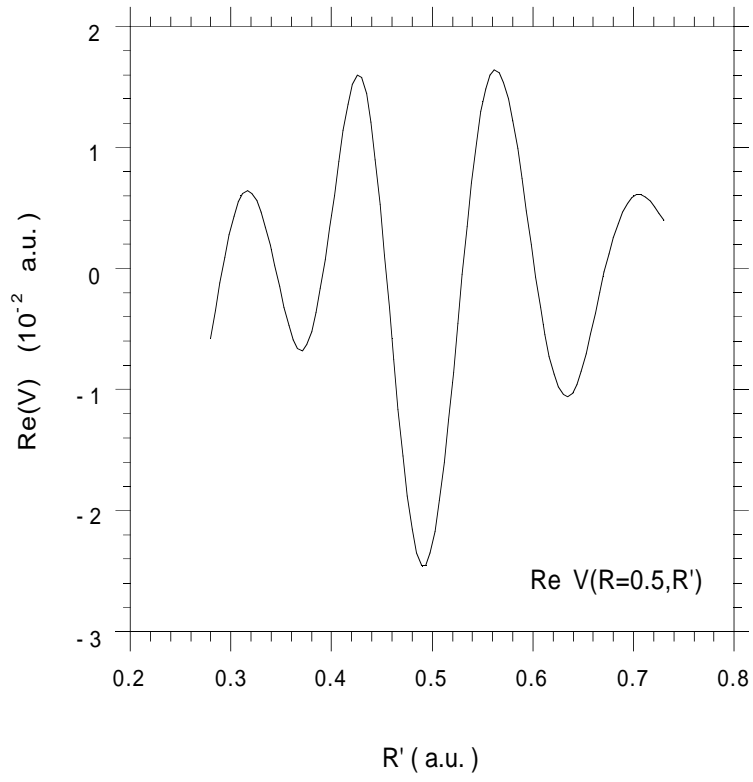


FIG. 3. Real part of effective potential $V_{eff}(R = 0.5, R')$

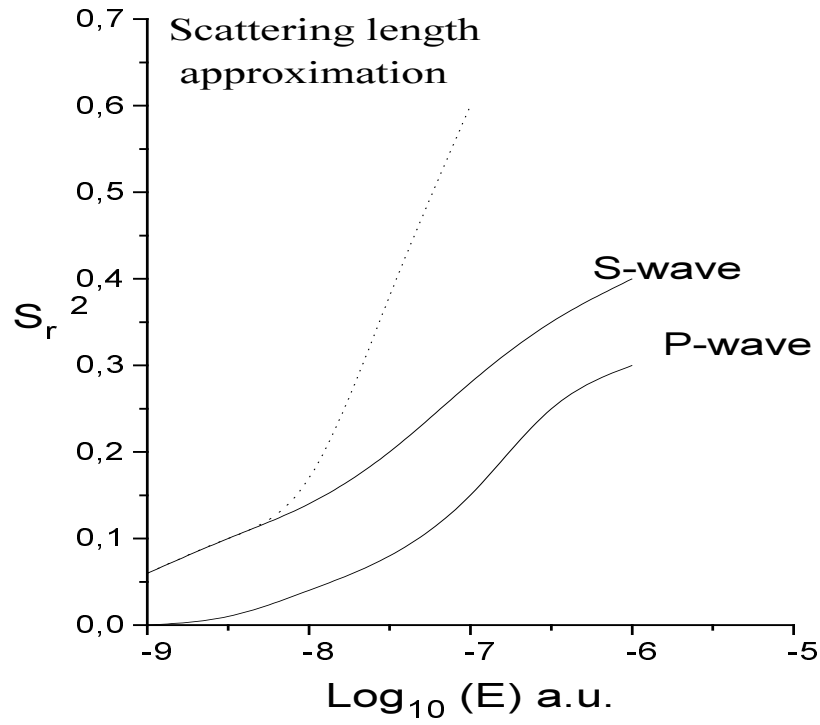


FIG. 4. Inelasticity $S_r = 1 - |S|^2$ for the $H + \bar{p} \rightarrow Pn^* + e$ reaction

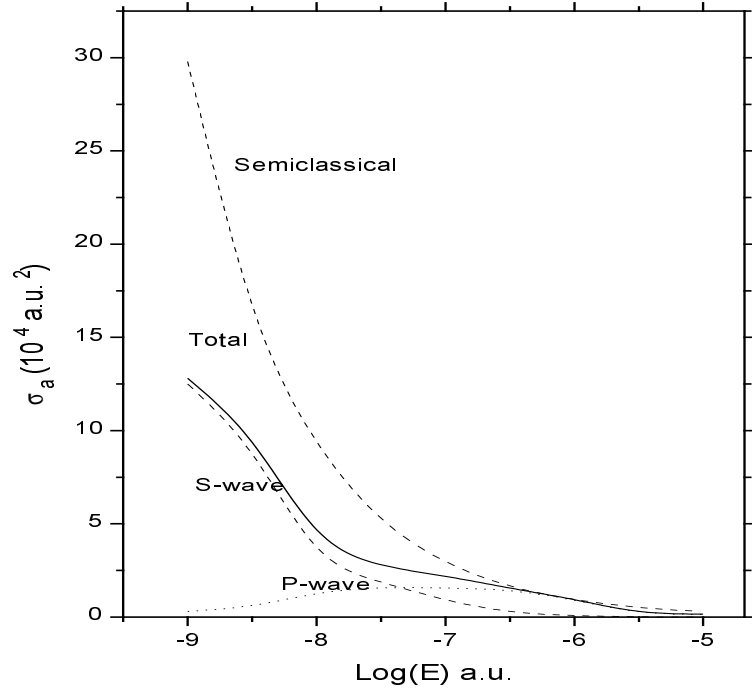


FIG. 5. Annihilation cross section for $H + \bar{p} \rightarrow Pn^* + e$

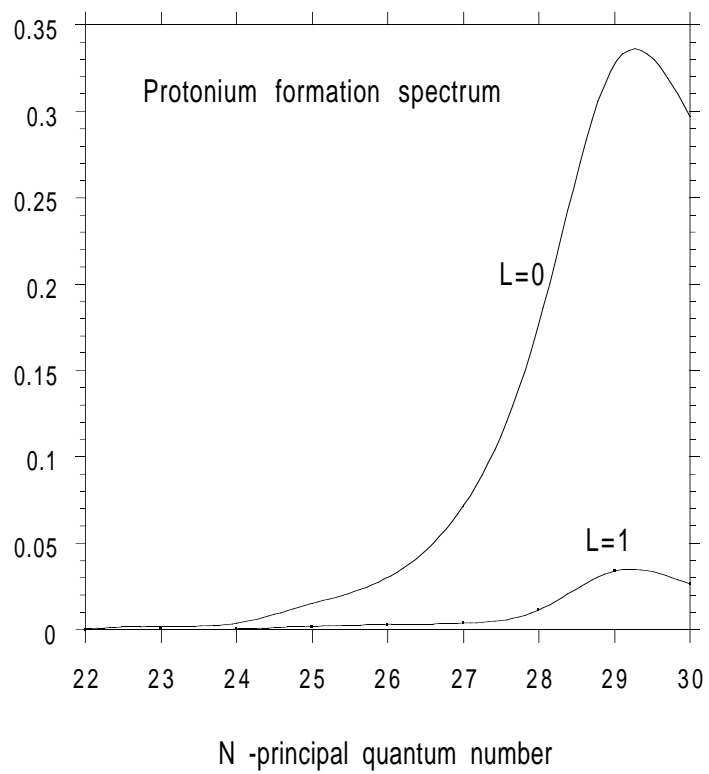


FIG. 6. Protonium formation probabilities in states with different quantum numbers

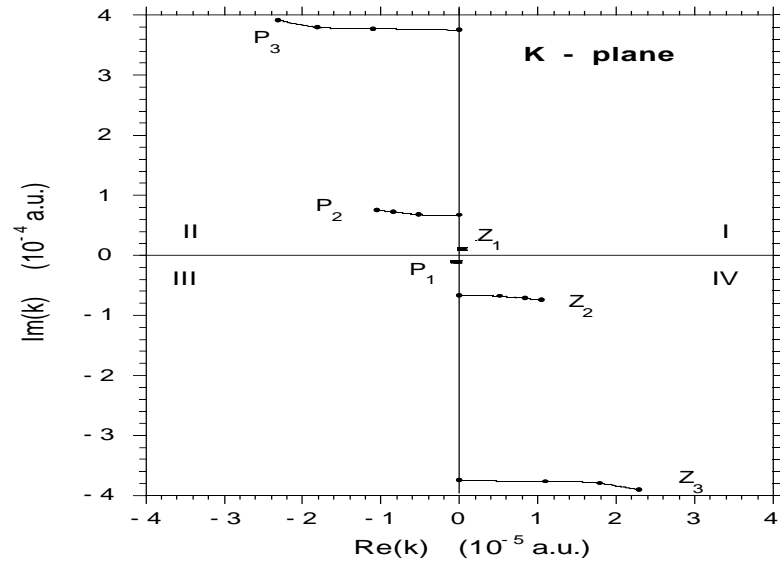


FIG. 7. S-matrix nearthreshold zeros (Z_i) and poles (P_i)

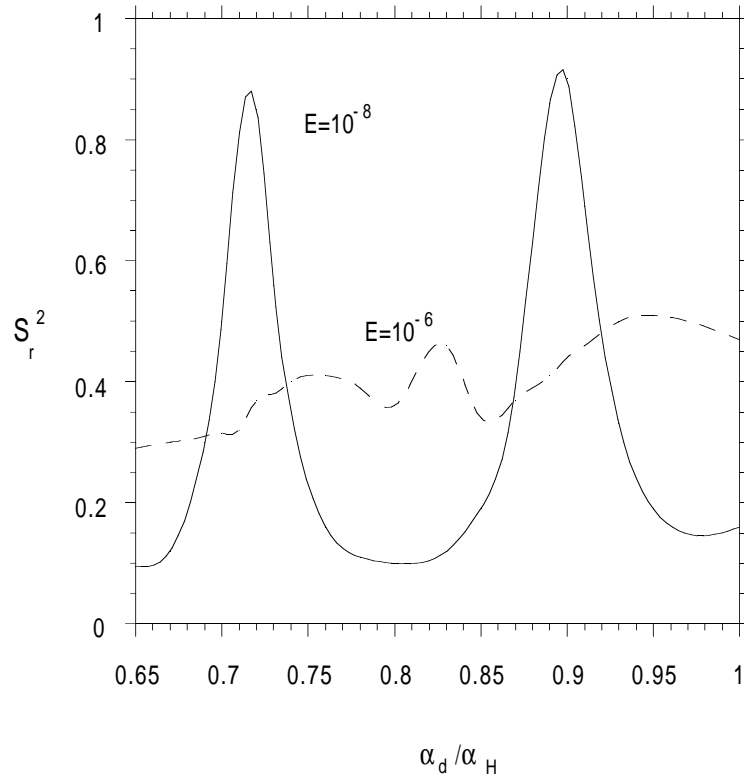


FIG. 8. Inelasticity for reaction $H + \bar{p} \rightarrow Pn^* + e$ as a function of the dipole polarizability α_d

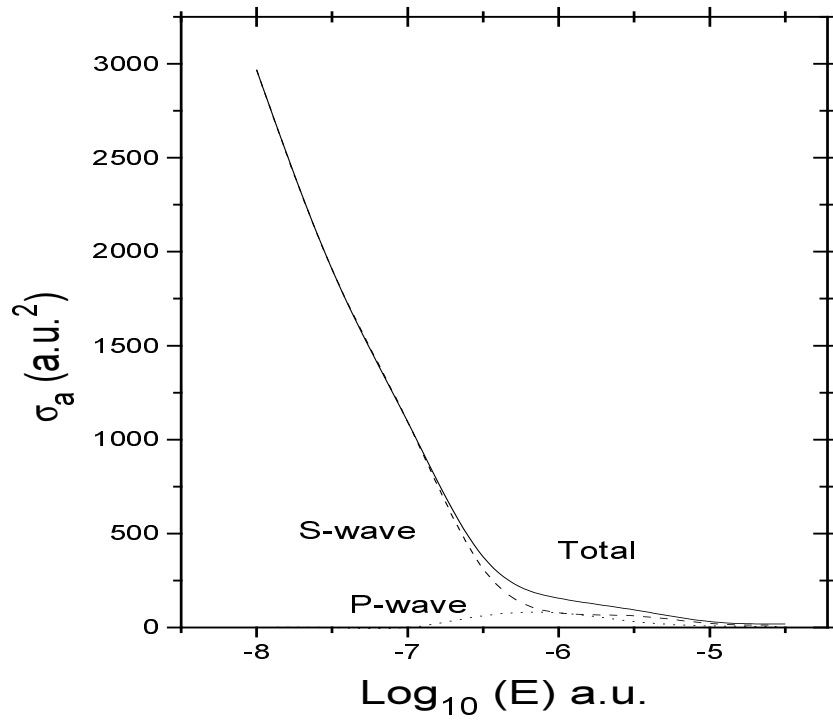


FIG. 9. Probability of reaction $H + \bar{H} \rightarrow Pn^* + (e^+e^-)$